Hole energy structure of multishell nanocrystals in a magnetic field

2002 J. Phys.: Condens. Matter 14 12537

(http://iopscience.iop.org/0953-8984/14/47/326)

INSTITUTE OF PHYSICS PUBLISHING JOURNAL OF PHYSICS: CONDENSED MATTER

J. Phys.: Condens. Matter **14** (2002) 12537–12549 PII: S0953-8984(02)34985-3

Hole energy structure of multishell nanocrystals in a magnetic field

J Planelles[1], **J Climente**[1], **J G Díaz**[1] **and W Jaskólski**[2]

[1] Departament de Ciències Experimentals, UJI, Box 224, E-12080, Castelló, Spain
[2] Instytut Fizyki UMK, Grudziądzka 5, 87-100 Toruń, Poland

Received 18 March 2002
Published 15 November 2002
Online at stacks.iop.org/JPhysCM/14/12537

Abstract

The influence of a magnetic field on the hole energy spectra of uniform and multilayer semiconductor nanocrystals is studied. The calculations are performed within the $\boldsymbol{k} \cdot \boldsymbol{p}$ method and envelope function approximation. The valence subband mixing is taken into account by considering a four-band Hamiltonian. It is found that the influence of a magnetic field depends strongly on the nanocrystal size and composition. Several phenomena, reported recently for electrons in multishell nanocrystals in a magnetic field, like crossover from confinement in the external shell to the internal core in quantum dot quantum barrier structures or spatial polar separation of the charge density in quantum dot quantum well systems, are also observed for holes. The calculated optical electron–hole transitions in small uniform spherical nanocrystals reveal that the δ_{lL}, selection rule, forbidding at $B = 0$ electron–hole transitions between states of different orbital angular momentum, is also approximately fulfilled, even at strong magnetic fields.

1. Introduction

Zero-dimensional semiconductor nanostructures have been intensively studied for the last two decades [1]. Different techniques for the fabrication of quantum dots allow for far-reaching manipulation of their sizes, shapes and compositions. To a large extent this permits the tailoring of their discrete energy levels and consequently their electronic and optical properties.

Of special interest is the investigation of magnetic field effects in such systems. This is because the weaker quantum confinement and lighter electron effective mass than in atomic physics makes it possible to observe effects that, for natural atoms, would require magnetic fields many orders of magnitude stronger than those accessible in the laboratory [1–5].

The ease of fabrication of quasi-two-dimensional quantum dots (by techniques of deep etching or electrostatic confinement applied to thin quantum wells or doped interfaces) and its close relation to the quantum Hall effect has resulted in magnetic field studies being almost exclusively limited to such systems [1]. Two-dimensional systems offer additional facilities

when the magnetic field is perpendicular to the structure and confinement is modelled by a parabolic potential. It has to be noticed that, since transport and capacitance spectroscopy experiments have been most widely used in the experimental study of the energy structure of single- and many-electron 2D quantum dots, the electron states have mostly been modelled theoretically.

Very little has been done so far in the study of the influence of a magnetic field on three-dimensional quantum dots. Some of them, like semiconductor nanocrystals grown in colloidal solutions by methods of wet chemistry, are particularly interesting. They can be synthesized as multishell nanocrystals, i.e. built of concentric layers (shells) of different semiconductors with the shell thickness down to a single monolayer [6–9]. In such structures, electrons and holes can be localized within very thin spherical-like wells, which greatly enhances the possibilities of tailoring their optical spectra. Recently, an interesting phenomenon of the transformation of electron resonant states of multilayer nanocrystals into bound states under the influence of a magnetic field has been reported [2, 3]. An exhaustive study of the magnetic field effects on the electron states of such nanocrystals has also been carried out very recently [10].

In this paper we study the influence of a magnetic field on the hole energy levels of uniform and multishell nanocrystals. To account for the valence subband mixing all the calculations are performed using the four-band $\boldsymbol{k}\cdot\boldsymbol{p}$ Hamiltonian. For very high magnetic fields the eight-band model should probably be more suitable. However, since the split-off band is separated from the heavy and light hole band by about 400 meV, it is reasonable to analyse the topmost valence discrete energy levels in the presence of a magnetic field by employing the four-band model as we do in the present paper.

Since the hole states are determined by the coupling of the p-type Bloch factors with envelope functions (defined by the nanocrystal shape and external field), the hole energy spectrum is usually denser than the electron one, with the states of high total angular momentum being energetically close to the ground state. We show that, unlike the electron case, the symmetry of the hole ground state of large nanocrystals changes rapidly with increasing magnetic field. We demonstrate that several interesting phenomena, like crossover from confinement in the external shell to the internal core in quantum dot quantum barrier systems or spatial polar separation of the single-particle charge density in quantum dot quantum well (QDQW) structures, found previously for electron states occur also for hole states.

For uniform quantum dots we also present preliminary results of calculations of the electron–hole transition rates. In multishell structures the field dependence of the electron [10] and hole energy levels and thus of optical transitions is less trivial and requires a separate investigation that is beyond the scope of this paper.

2. Theory and computational details

Let us consider the four-band $\boldsymbol{k}\cdot\boldsymbol{p}$ Hamiltonian that couples the heavy hole and light hole subbands [11]. This Hamiltonian, represented in the conventional Luttinger–Kohn basis $|J, J_z\rangle$ [12], is

	$\lvert 3/2, 3/2\rangle$	$\lvert 3/2, 1/2\rangle$	$\lvert 3/2, -1/2\rangle$	$\lvert 3/2, -3/2\rangle$
$\lvert 3/2, 3/2\rangle$	$-(P+Q)$	$-\mathrm{i}L$	$-M$	0
$\lvert 3/2, 1/2\rangle$	$\mathrm{i}L^*$	$-(P-Q)$	0	$-M$
$\lvert 3/2, -1/2\rangle$	$-M^*$	0	$-(P-Q)$	$\mathrm{i}L$
$\lvert 3/2, -3/2\rangle$	0	$-M^*$	$-\mathrm{i}L^*$	$-(P+Q)$

(1)

When zero-dimensional nanostructures are considered, in which the holes can be totally confined in three dimensions, the envelope function approximation is applied and the elements

of the Hamiltonian become the operators acting on the components, f_i, of the envelope function of $\Psi = \sum u_i f_i$. In the spherical approximation these operators are (in atomic units)

$$\begin{aligned} &P = \frac{\gamma_1}{2}p^2, \qquad Q = \frac{\gamma}{2}(p_\perp^2 - 2p_z^2), \qquad L = -\mathrm{i}\sqrt{3}\gamma p_z p_-, \\ &M = \frac{\sqrt{3}\gamma}{2}p_-^2, \qquad p_\pm = p_x \pm \mathrm{i}p_y, \qquad p_\perp^2 = p_x^2 + p_y^2, \\ &p^2 = p_\perp^2 + p_z^2, \qquad p_\alpha = -\mathrm{i}\nabla_\alpha, \end{aligned} \tag{2}$$

where γ, γ_1 are Luttinger parameters [12], $\alpha = x$, y or z, and u_i are the Bloch functions.

When there is no magnetic field, this Hamiltonian is usually written in spherical coordinates and results in two coupled differential equations in the radial variable [12]. In such a case the valence band states are labelled by nQ_F, where Q denotes the spectroscopic notation for the lowest value of the envelope angular quantum number L in the wavefunction Ψ; F is the quantum number of the total angular momentum $\boldsymbol{F} = \boldsymbol{L} + \boldsymbol{J}$, where $\boldsymbol{J}$ is the Bloch angular momentum, $J = 3/2$, and n labels consecutive states of a given Q and F.

When the external magnetic field is applied the spherical symmetry is broken and the Hamiltonian (derived in cylindrical coordinates) commutes only with the operator $\boldsymbol{F}_z$ of the projection of $\boldsymbol{F}$ onto the field axis. The states are labelled by F_z. To identify these states by their spherical notation at $B = 0$ we have performed, for $B = 0$, two sets of calculations in both coordinates. This allows us to label the states, in cylindrical coordinates, as nQ_F, F_z.

For $B \neq 0$ the axial approximation could be used to derive the Hamiltonian in cylindrical coordinates. However, for a more adequate comparison with the results obtained for $B = 0$, the so-called spherical approximation with only two Luttinger parameters is employed in all the cases.

Transforming the Hamiltonian to cylindrical coordinates (ρ, z, ϕ) and integrating over the ϕ angle yields four coupled differential equations (see table 1) for the envelope function components (i) $f_M^i(\rho, z)$ [13]. The diagonal elements of the equations in table 1 include the potential energy $V(\rho, z)$, that depends on the actual geometry, composition and structure of the studied system, and the interaction with an external uniform magnetic field[3] $\boldsymbol{B} = (0, 0, B)$.

In looking for the bound states of the investigated systems all the envelope function components are required to vanish for large ρ and z. For multishell structures, V is formed by the valence band off-sets. Since the hole effective masses and thus γ, γ_1 parameters are different in different layers, appropriate matching conditions should in general be applied at the corresponding interfaces. In this paper, for simplicity, uniform Luttinger parameters are considered for all the investigated systems.

The equations presented in table 1 have been solved numerically using the finite-difference method on a two-dimensional grid (ρ, z) in cylindrical coordinates. The discretization of the differential equations yields eigenvalue problems of asymmetric huge and sparse matrices that have been solved by the iterative Arnoldi solver [14] implemented in the ARPACK package [15].

Optical transition rates between the conduction and valence-band states are calculated excluding exciton effects. Including Coulomb interaction yields just a parallel rearrangement of the spectrum (see, e.g., [16]), after a far more complex calculation. In cylindrical coordinates the electron $\Psi_{F_z}^e$ and hole $\Psi_{F_z}^h$ wavefunctions can be written as

$$\Psi_{F_z}^e = f_m^e(\rho, z)\mathrm{e}^{\mathrm{i}m\phi}|S, \sigma\rangle, \tag{3}$$

[3] Magnetic field enters the diagonal terms of the multiband Hamiltonian as $-\frac{F_z B}{2m^*} - \frac{B^2\rho^2}{8m^*}$, where m^* is the heavy-hole or light-hole effective mass and F_z is the quantum number of F_z. One could consider a magnetic field present also in off-diagonal elements due to the term $\boldsymbol{A}\cdot\boldsymbol{p}$, where $\boldsymbol{A} = (-y/2, x/2, 0)B$ is the vector potential. The preliminary analysis shows, however, that the results will not differ significantly.

Table 1. Two-band $\boldsymbol{k}\cdot\boldsymbol{p}$ Hamiltonian in cylindrical coordinates.

$\frac{(\gamma+\gamma_1)}{2}\left[\frac{\partial^2}{\partial\rho^2}+\frac{1}{\rho}\frac{\partial}{\partial\rho}-\frac{(F_z-1.5)^2}{\rho^2}\right]+\frac{(\gamma_1-2\gamma)}{2}\frac{\partial^2}{\partial z^2}-(\gamma_1-2\gamma)\left[\frac{B^2\rho^2}{8}+\frac{F_zB}{2}\right]+V(\rho,z)$	$\sqrt{3}\gamma\left[\frac{\partial^2}{\partial\rho\partial z}+\frac{F_z-0.5}{\rho}\frac{\partial}{\partial z}\right]$	$-\sqrt{3}\frac{\gamma}{2}\left[\frac{\partial^2}{\partial\rho^2}+\frac{2F_z}{\rho}\frac{\partial}{\partial\rho}+\frac{F_z(F_z-1)-0.75}{\rho^2}\right]$	0
$\sqrt{3}\gamma\left[\frac{\partial^2}{\partial\rho\partial z}-\frac{F_z-0.5}{\rho}\frac{\partial}{\partial z}\right]$	$\frac{(\gamma_1-\gamma)}{2}\left[\frac{\partial^2}{\partial\rho^2}+\frac{1}{\rho}\frac{\partial}{\partial\rho}-\frac{(F_z-0.5)^2}{\rho^2}\right]+\frac{(\gamma_1+2\gamma)}{2}\frac{\partial^2}{\partial z^2}-(\gamma_1+2\gamma)\left[\frac{B^2\rho^2}{8}+\frac{F_zB}{2}\right]+V(\rho,z)$	0	$-\sqrt{3}\frac{\gamma}{2}\left[\frac{\partial^2}{\partial\rho^2}+\frac{2(F_z+1)}{\rho}\frac{\partial}{\partial\rho}+\frac{F_z(F_z+1)-0.75}{\rho^2}\right]$
$-\sqrt{3}\frac{\gamma}{2}\left[\frac{\partial^2}{\partial\rho^2}-\frac{2(F_z-1)}{\rho}\frac{\partial}{\partial\rho}+\frac{F_z(F_z-1)-0.75}{\rho^2}\right]$	0	$\frac{(\gamma_1-\gamma)}{2}\left[\frac{\partial^2}{\partial\rho^2}+\frac{1}{\rho}\frac{\partial}{\partial\rho}-\frac{(F_z+0.5)^2}{\rho^2}\right]+\frac{(\gamma_1+2\gamma)}{2}\frac{\partial^2}{\partial z^2}-(\gamma_1+2\gamma)\left[\frac{B^2\rho^2}{8}+\frac{F_zB}{2}\right]+V(\rho,z)$	$-\sqrt{3}\gamma\left[\frac{\partial^2}{\partial\rho\partial z}+\frac{F_z+1.5}{\rho}\frac{\partial}{\partial z}\right]$
0	$-\sqrt{3}\frac{\gamma}{2}\left[\frac{\partial^2}{\partial\rho^2}-\frac{2F_z}{\rho}\frac{\partial}{\partial\rho}+\frac{F_z(F_z+1)-0.75}{\rho^2}\right]$	$-\sqrt{3}\gamma\left[\frac{\partial^2}{\partial\rho\partial z}-\frac{F_z+0.5}{\rho}\frac{\partial}{\partial z}\right]$	$\frac{(\gamma+\gamma_1)}{2}\left[\frac{\partial^2}{\partial\rho^2}+\frac{1}{\rho}\frac{\partial}{\partial\rho}-\frac{(F_z+1.5)^2}{\rho^2}\right]+\frac{(\gamma_1-2\gamma)}{2}\frac{\partial^2}{\partial z^2}-(\gamma_1-2\gamma)\left[\frac{B^2\rho^2}{8}+\frac{F_zB}{2}\right]+V(\rho,z)$

$$\Psi^h_{F_z}=\sum_{M=F_z-3/2}^{F_z+3/2} f^h_M(\rho,z)\mathrm{e}^{\mathrm{i}M\phi}|3/2,(F_z-M)\rangle, \tag{4}$$

where $|S,\sigma\rangle$ and $|3/2,(F_z-M)\rangle$ are the electron and hole Bloch functions, respectively, $\sigma=\pm1/2$, and $(m+\sigma)=F_z$. The optical transition matrix element

$$\begin{aligned}|\langle\Psi^e_{F'_z}|\boldsymbol{p}|\Psi^h_{F_z}\rangle|^2&=\left|\sum_M\int f^e_m f^h_M\rho\,\mathrm{d}\rho\,\mathrm{d}z\,\delta_{mM}\langle S,\sigma|\boldsymbol{p}|3/2,(F_z-M)\rangle\right|^2\\&=S^2_{eh}|\langle S,\sigma|\boldsymbol{p}|3/2,(F_z-m)\rangle|^2\delta_{mM}\end{aligned} \tag{5}$$

is a product of the electron–hole overlap S^2_{eh} and the angular part. The δ_{mM} symbol has been kept in equation (5) to make sure that the transition is forbidden when m is different from any M in the sum. The angular factor is calculated in terms of the square of the Kane parameter $P^2=|\langle S|p_x|X\rangle|^2$, after explicitly writing the Bloch factors in terms of the eight band-edge basis functions $\{|S,1/2\rangle,|S,-1/2\rangle,|X,1/2\rangle,\ldots,|Z,-1/2\rangle\}$ [17].

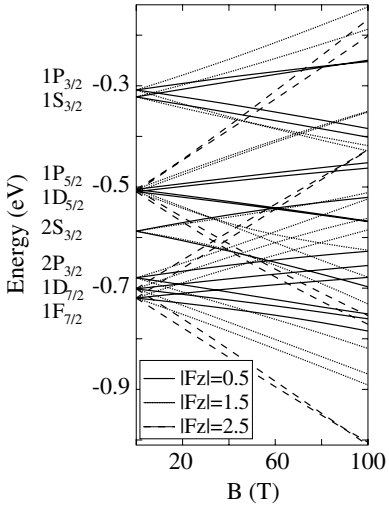

Figure 1. Hole energy levels, nQ_F, for a uniform InAs nanocrystal of diameter $d = 6$ nm versus magnetic field. Only components $|F_z| = 0.5$ (full line), $|F_z| = 1.5$ (dotted line) and $|F_z| = 2.5$ (broken line) are shown.

3. Results

3.1. Uniform nanocrystal

Although the main aim of this paper is the study of the influence of a magnetic field on the energy structure of multishell nanocrystals, for the sake of comparison we also include some results for uniform nanocrystals [10]. We consider InAs nanocrystals. They can be grown by methods of wet chemistry as clusters of almost spherical shapes and sizes of 2–10 nm [18]. In our formulation they are modelled by a finite spherical rectangular potential well (4 eV). Luttinger parameters, $\gamma_1 = 19.7$ and $\gamma = 8.4$, corresponding to heavy hole and light hole effective masses $m_{hh} = 0.345$ and $m_{lh} = 0.027$, are used [19].

We investigate the influence of a magnetic field on the hole energy spectra of two different InAs nanocrystals of radii 3 and 8 nm. The results are shown in figures 1 and 3(c), respectively. In the absence of a magnetic field the energies of the ground and first excited states are very close: for the smaller nanocrystal the ground state is $1P_{3/2}$, while for the large one it is $1S_{3/2}$. The field dependence of the hole energy levels for the smaller nanocrystal (figure 1) is almost linear in the whole range of the magnetic field investigated. The quadratic term in the Hamiltonian (table 1) becomes significant for the larger nanocrystal (see figure 3(c)).

Since the linear term is proportional to F_z, the higher F_z the lower the relative weight of the quadratic term to the linear one. Thus, for the states of $F_z = \pm\frac{1}{2}$ the quadratic term becomes significant even at laboratory fields, while for the states of $|F_z| = \frac{5}{2}$, the linear term is still dominant even at fields as strong as 50 T. It is the ratio $t = \rho_o/r_{max}$ between the radius of the maximum charge density in the lowest Landau orbit, ρ_0, and the radius of the maximum charge density in a given state, r_{max}, that decides whether only the linear Zeeman term or also the quadratic term in the Hamiltonian (table 1) is observed. If $t > 1$ then only the linear term is significant.

For the hole states the Landau levels, and thus the corresponding Landau orbits, are not well defined, since the heavy-hole and light-hole subbands are mixed even at strong magnetic fields. One can, however, estimate ρ_0 as $[(2|F_z| + 1)\frac{\hbar}{eB}]^{1/2}$ [2]. Since for the states with

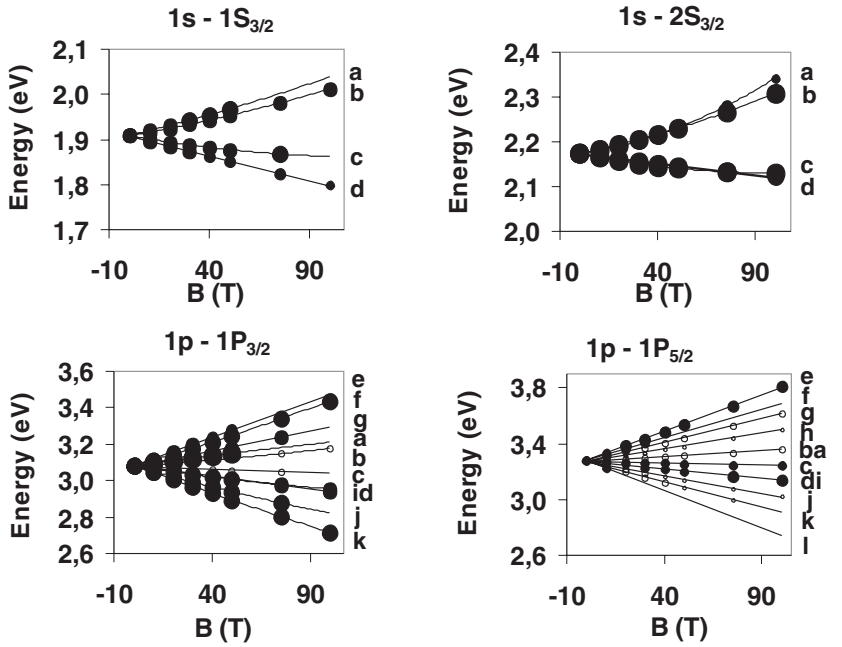

Figure 2. Electron–hole, $m \rightarrow F_z$, optical transition rates for a uniform InAs nanocrystal of diameter $d = 6$ nm. $m = 0$: $F_z = 1.5$ (a), $F_z = 0.5$ (b), $F_z = -0.5$ (c), $F_z = -1.5$ (d) ; $m = 1$: $F_z = 2.5$ (e), $F_z = 1.5$ (f), $F_z = 0.5$ (g), $F_z = -0.5$ (h); $m = -1$: $F_z = 0.5$ (i), $F_z = -0.5$ (j), $F_z = -1.5$ (k), $F_z = -2.5$ (l). For the overlapping spots the order corresponds to the transition strengths. The spot size is proportional to the calculated transition moment.

$|F_z| = 1/2$, $\rho_0 > 3$ nm (even at $B = 100$ T), only the linear term is significant for these states in the case of the smaller nanocrystal. All the same, $\rho_0 = 7$ nm at $B = 25$ T and this explains why the quadratic term becomes significant for the larger quantum dot.

Several anticrossings that are seen in figure 3(c) come from a different evolution (in the magnetic field) of the states of a given F_z, having for $B = 0$ a different number of nodes. A closer inspection of figures 1 and 3(c) shows that the splitting of the energy levels belonging to a given pair $\pm F_z$ can be very different for the pairs of states of the same $|F_z|$. It can also happen that the splitting of pairs belonging to different F_z is very similar. $\mathrm{E}(2\mathrm{S}_{3/2}, +\frac{1}{2}) - \mathrm{E}(2\mathrm{S}_{3/2}, -\frac{1}{2})$ and $\mathrm{E}(2\mathrm{S}_{3/2}, +\frac{3}{2}) - \mathrm{E}(2\mathrm{S}_{3/2}, -\frac{3}{2})$ is one of the examples. This behaviour is a consequence of a strong heavy-hole and light-hole subband mixing.

The optical transition rates for transitions between the lowest conduction band and the highest valence band states for the case of the smaller nanocrystal are shown in figure 2. At $B = 0$, the δ_{mM} selection rule (see equation (5)) must be supplemented by $\delta_{l\,L}$ [20], where l, L are the orbital angular momentum quantum numbers of the electron wavefunctions and hole wavefunction components, respectively. In the presence of a magnetic field, the spherical symmetry is broken: l and L are no longer good quantum numbers. However, the calculated matrix elements of transitions that are forbidden at $B = 0$ (like $1\mathrm{s}-1\mathrm{P}_{3/2}$, $1\mathrm{s}-1\mathrm{P}_{5/2}$, $1\mathrm{p}-1\mathrm{S}_{3/2}$, etc) are very small even at magnetic fields as strong as 50 T. These transitions are not shown in figure 2. When the magnetic field is about 60 T some of the strong transitions become negligible. It happens, for example, to the component $m = 0$ to $F_z = 1.5$ of the transition $1\mathrm{s} \rightarrow 1\mathrm{S}_{3/2}$ (see '*a*' at the top left part of figure 2). Simultaneously the same component of the transition $1\mathrm{s} \rightarrow 1\mathrm{P}_{3/2}$, negligible below $B = 60$ T, becomes very strong. This is due to

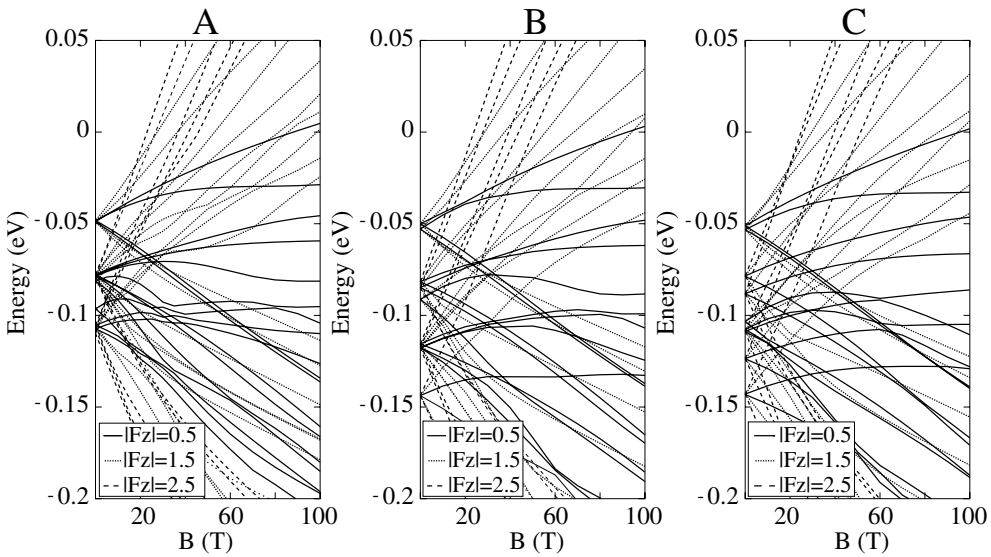

Figure 3. Hole energy levels versus magnetic field of (A) a spherical multilayer InAs(7 nm)/InP(1 nm)/InAs(3.5 nm) QDQB, (B) the same as A but with a 2 nm external InAs cladding and (C) a uniform InAs nanocrystal of diameter $d = 16$ nm.

the anticrossing of the hole states $1P_{3/2}(F_z = 1.5)$ and $1S_{3/2}(F_z = 1.5)$ that happens about this field (see figure 1), where the states exchange their wavefunctions.

3.2. Quantum dot quantum barrier (QDQB)

In this section we consider three-layer nanocrystals built of an internal InAs core of radius 7 nm, a middle InP shell of thickness 1 nm and an external InAs cladding. Two different nanocrystals having an external InAs cladding of thickness 2 and 3.5 nm have been studied. Since the forbidden energy gap of InAs is narrower than the gap of InP, the middle shell acts as a 0.42 eV barrier separating two spherical InAs wells [18]. The surrounding medium is modelled by a 4 eV external potential barrier. Since we are mainly interested in the states having energies below the InP barrier and thus small charge density in the barrier region, the Luttinger parameters of InAs are used in the whole nanocrystal.

The energy levels closest to the top of the InAs valence band edge ($F_z = \pm 0.5, \pm 1.5, \pm 2.5$) of the two studied nanocrystals versus magnetic field are presented in figure 3. The energy levels of the homogeneous InAs QD of radius 8 nm are shown for comparison. For $B = 0$, a rearrangement of some energy levels with increasing thickness of the external cladding, reported previously for electrons [10], is also observed here. The states having radial nodes are favourable for building a significant charge density in the external cladding in comparison to the nodeless states. This is illustrated in figure 4, where the contours of the charge densities (in the absence of magnetic field) of the $2S_{3/2}$, $2P_{3/2}$ and $3S_{3/2}$ states corresponding to the nanocrystal with thicker external cladding are shown. The $2S_{3/2}$ state builds a large part of the density in the internal core, while $2P_{3/2}$ and $3S_{3/2}$ states have most of their density localized in the external cladding.

Figure 3 shows that, except for $F_z = \pm 0.5$, the field dependence of the energy levels of the studied nanocrystals is nearly linear. In both cases many anticrossings can be seen.

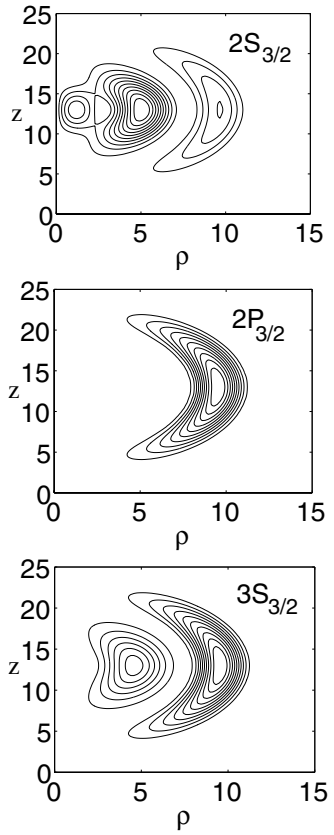

Figure 4. Charge density contours of $2S_{3/2}$, $2P_{3/2}$ and $3S_{3/2}$ hole states of a spherical multishell InAs(7 nm)/InP(1 nm)/InAs(3.5 nm) QDQB.

The magnetic confinement is more pronounced for the $F_z = \pm 0.5$ states, since the radius of the maximum charge density in the corresponding lowest Landau level is the smallest. The magnetic confinement is particularly strong for the nodal states of the nanocrystal having the thicker external clad, like the $2P_{3/2}$ and $3S_{3/2}$ states, that can build most of their charge density in the external cladding (see figure 4). These states show the most pronounced quadratic field dependence and are responsible for many anticrossings that happen even at low magnetic field (figure 5). A crossover from confinement in the external shell to the internal core produced by the magnetic field, reported previously for electron states [10], is also observed for the hole states.

Since the field dependence of the energy levels with $|F_z| \geqslant 3/2$ is almost linear, it happens that the excited states with very high negative z components of the angular momentum turn into the ground state when the magnetic field increases. We have calculated this dependence for F_z up to $-41/2$. In figure 6 several energy levels with high F_z versus magnetic field, for the nanocrystal with the thicker external cladding, are shown. The $F_z = -3/2$ component of $P_{3/2}$ is the ground state up to the magnetic field of about 13 T. Then, the state of $F_z = -19/2$ becomes the ground state; next $F_z = -27/2$, and later, at about 20 T, $F_z = -33/2$ (which is already unbound at $B = 0$ T). For the quantum barrier nanocrystal with the thinner external cladding and for the homogeneous InAs nanocrystal this behaviour is similar, although it happens at higher magnetic fields.

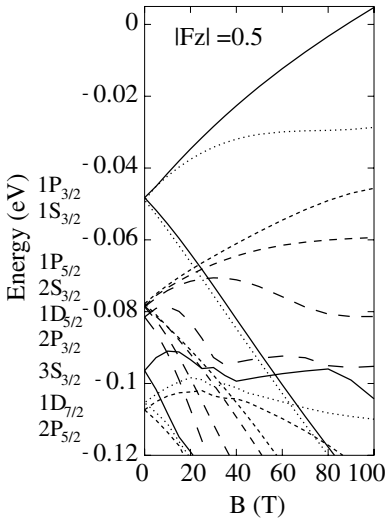

Figure 5. Hole energy levels versus magnetic field, $|F_z| = 0.5$, components of a spherical multishell InAs(7 nm)/InP(1 nm)/InAs(3.5 nm) QDQB nanocrystal.

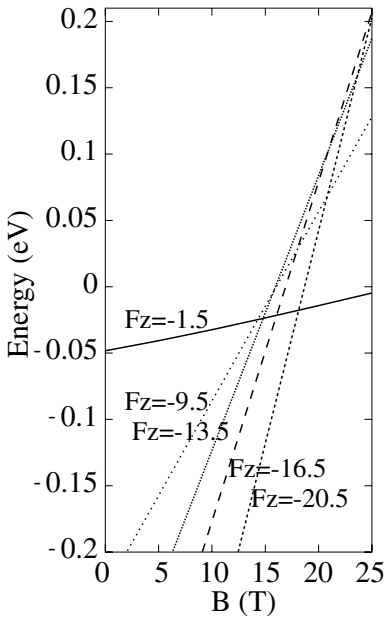

Figure 6. Ground state energy and symmetry changes versus magnetic field for a multishell InAs(7 nm)/InP(1 nm)/InAs(3.5 nm) QDQB nanocrystal.

3.3. Quantum dot quantum well

Let us consider now a three-layer nanocrystal built of an internal barrier-acting InP core, a middle well-acting InAs shell and an external barrier-acting InP cladding. The radius of the core is 8 nm, the thickness of the InAs and InP shells is 2 nm, the conduction band offset is 0.42 eV [18] and the height of the surrounding barrier is assumed as 4 eV (from the bottom of

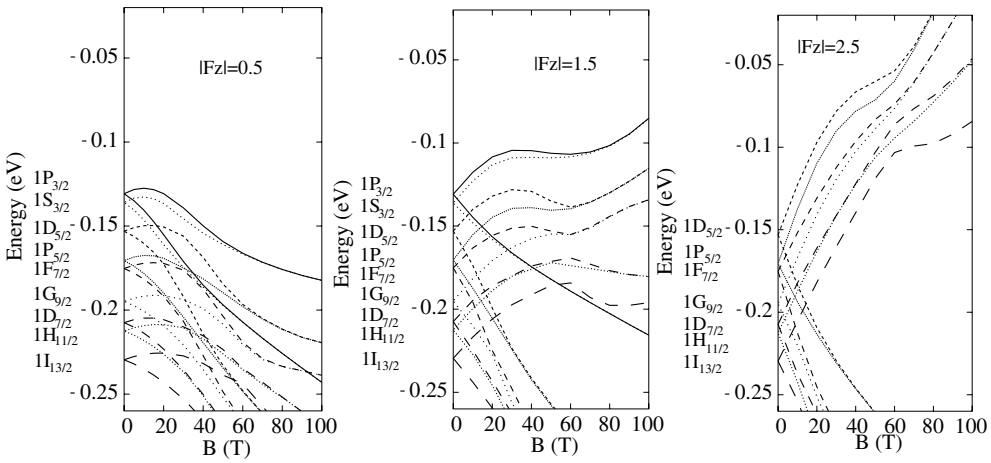

Figure 7. Hole energy levels versus magnetic field of a spherical multilayer InP(8 nm)/InAs(2 nm)/InP(2 nm) QDQW nanocrystal.(A) $|F_z| = 0.5$, (B) $|F_z| = 1.5$ and (C) $|F_z| = 2.5$ components.

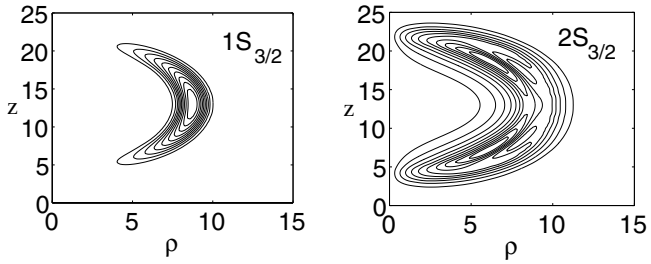

Figure 8. Charge density contours of the $1S_{3/2}$ and $2S_{3/2}$ hole states of a QDQW nanocrystal.

the InAs well). Since we are investigating the bound states having charge densities localized mainly in the middle shell, the valence band Luttinger parameters of InAs are used in the whole structure ($\gamma = 8.4$ and $\gamma_1 = 19.7$).

In figure 7 the lowest energy levels for $F_z = \pm 0.5, \pm 1.5$ and ± 2.5 versus the magnetic field are presented. In contrast to what has been observed for the QDQB systems, the energies of all the states of the QDQW structure show a quadratic field dependence, even at a relatively weak magnetic field. This behaviour is similar to that observed in quantum rings [4, 13]. In both cases the wavefunction of the first state of each symmetry has most of its density localized in the well or ring (see figure 8). The radius of the maximum of its radial density is, even at low fields, larger than the radius of the maximum charge density in the lowest Landau level. This causes a strong enhancement of the quadratic dependence of the energy levels on the magnetic field.

Comparing the hole energy spectra of the QDQW (figure 7) and QDQB (figure 5) systems, one can see the absence of the second state of each symmetry in the case of QDQW within the energy plot range. This effect can be easily explained: in the case of the QDQB, the second state of each symmetry has a nodal surface in the barrier region. As a consequence its charge density can localize freely in an internal and/or external InAs well, not leading to any extra increase of the energy. In the case of the QDQW, the nodal surface is located in a rather thin

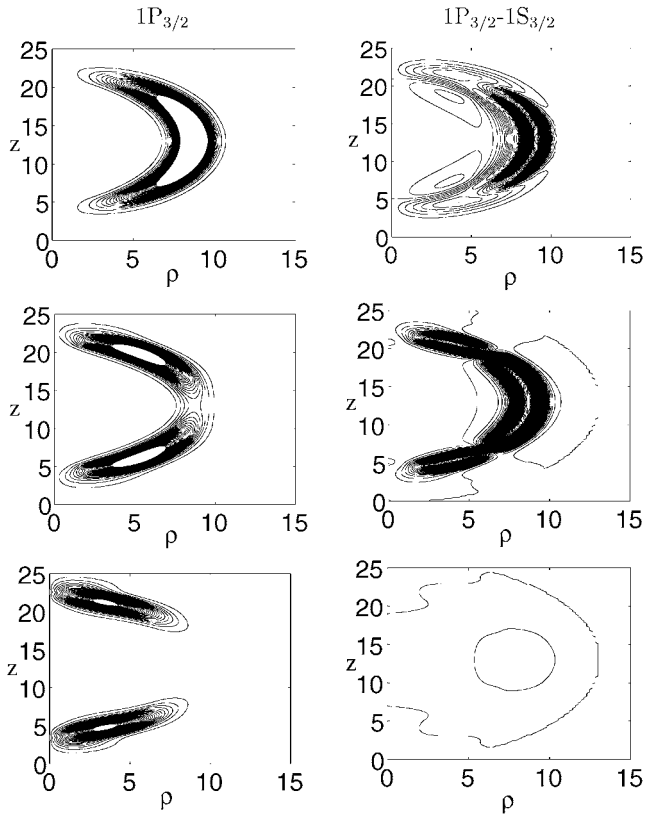

Figure 9. Charge density contours of the $1P_{3/2}$ hole state and density differences ($1P_{3/2} - 1S_{3/2}$) for a QDQW nanocrystal. Magnetic fields: $B = 0$, 50 and 100 T (from top to bottom).

InAs well, so that the charge density has to localize outside of the well, leading to an increase in the energy of this state (down from the InAs valence band edge). The lowest $n = 2$ state is $2D_{7/2}$ with the energy -0.307 eV.

Another interesting feature of this energy spectrum is that, as for electrons [10], the two consecutive states of the same F_z approach each other as the magnetic field increases. Thus, at high fields the spectrum consists of a series of two-fold quasi-degenerate energy levels. In figure 7 one can see how the pairs ($1P_{3/2}$, $1/2$, $1S_{3/2}$, $1/2$), ($1P_{3/2}$, $-1/2$, $1S_{3/2}$, $-1/2$), ($1P_{3/2}$, $3/2$, $1S_{3/2}$, $3/2$), ($1P_{3/2}$, $-3/2$, $1S_{3/2}$, $-3/2$), ($1D_{5/2}$, $5/2$, $1P_{5/2}$, $5/2$), ($1D_{5/2}$, $-5/2$, $1P_{5/2}$, $-5/2$), ($1D_{5/2}$, $3/2$, $1P_{5/2}$, $3/2$), ($1D_{5/2}$, $-3/2$, $1P_{5/2}$, $-3/2$), ($1D_{5/2}$, $1/2$, $1P_{5/2}$, $1/2$), ($1D_{5/2}$, $-1/2$, $1P_{5/2}$, $-1/2$), etc become quasi-degenerate at a high magnetic field. To understand these effects, the contours of the charge densities for the state $1P_{3/2}$, and the density difference of the $1P_{3/2}$ and $1S_{3/2}$ states, at $B = 0$, 50 and 100 T are plotted in figure 9. When the magnetic field increases, the difference in the charge densities of these two states drops down to zero. The increasing magnetic field tries to *squeeze* the charge into the small Landau orbit, but since it bounces the wide internal InP barrier, the charge concentrates finally in the two polar regions of the InAs well (see figure 9). In an extremely strong field, in which the Landau orbit is much smaller than the radius of the internal well, one can consider these pairs of states as *even* and *odd* solutions for a kind of almost 1D double well created by a cross section of the QDQW potential along the field axis. As an indirect consequence of this

singular behaviour of the energy levels, the number of anticrossings that occur in QDQW is much lower than in the QDQB or homogeneous nanocrystals.

Finally we point out that, similar to the QDQBs and homogeneous nanocrystals, the energy levels with very high $|F_z|$ values undergo a strong $\pm F_z$ splitting caused by the linear magnetic term in the Hamiltonian. This leads to sequential changes of the ground state symmetry as the magnetic field increases. However, these changes do not occur for consecutive values of F_z (unit by unit), as happens for the electron states in the QDQW [10] or for electron and hole states in quantum rings [13].

3.4. Concluding remarks

The influence of a magnetic field on the hole energy spectra of uniform and multishell nanocrystals has been studied. The results of calculations performed for quantum dot quantum barrier and QDQW structures reveal fundamental differences between barrier-like and well-like nanocrystals. Several interesting phenomena, like crossover from confinement in the external shell to the internal core (in QDQB systems) or spatial polar separation of single-particle charge density (in QDQW structures), are reported. Calculated optical transitions for small uniform spherical nanocrystals indicate that the selection rule δ_{lL}, which forbids electron–hole transitions between different angular momenta at $B = 0$, is also even approximately true in the presence of a strong magnetic field.

Acknowledgments

Financial support from DGESIC-P1B97-0397, UJI-P1B97-23, MSC Fund II and KBN-8T11B06218 is gratefully acknowledged. MCT-FPU (JC) and Generalitat Valenciana FPI grants (JD) are also acknowledged.

References

[1] For review see, e.g.,
Jacak L, Hawrylak P and Wójs A 1998 *Quantum Dots* (Berlin: Springer)
Chakraborty T 1999 *Quantum Dots* (Amsterdam: Elsevier)
[2] Bylicki M and Jaskólski W 1999 *Phys. Rev.* B **60** 15924
[3] Jaskólski W, Bosek M, Bylicki M and Planelles J 2001 *Vacuum* **63** 185
[4] Lorke A, Luyken R J, Govorov A O, Kotthaus J P, Garcia J M and Petroff P M 2000 *Phys. Rev. Lett.* **84** 2223
[5] Lieb E H, Solovej J P and Yngvason J 1995 *Phys. Rev.* B **51** 10646
[6] Mews A, Eychmüller A, Giersig M, Schoos D and Weller H 1994 *J. Phys. Chem.* **98** 934
[7] Mews A, Kadavanich A V, Banin U and Alivisatos A P 1996 *Phys. Rev.* B **53** R13242
[8] Little R B, El-Sayed M A, Bryant G W and Burke S 2001 *J. Chem. Phys.* **114** 1813
[9] Woggon U 1997 *Optical Properties of Semiconductor Quantum Dots* (Berlin: Springer)
[10] Planelles J, Diaz J, Climente J and Jaskólski W 2002 *Phys. Rev.* B **65** 245302
[11] Baldereschi A and Lipari N O 1973 *Phys. Rev.* B **42** 2697
Gregorian G B, Kazaryan E M, Efros Al L and Yazeva T V 1990 *Sov. Phys.–Solid State* **32** 1031
[12] Sercel P C and Vahala K J 1990 *Phys. Rev.* B **42** 3690
[13] Planelles J, Jaskólski W and Aliaga I 2001 *Phys. Rev.* B **65** 033306
[14] Arnoldi W E 1951 *Quart. J. Appl. Math.* **9** 17
Saad Y 1992 *Numerical Methods for Large Scale Eigenvalue Problems* (New York: Halsted)
Morgan R B 1996 *Math. Comput.* **65** 1213
[15] Lehoucq R B, Sorensen D C, Vu P A and Yang C *ARPACK: Fortran Subroutines for Solving Large Scale Eigenvalue Problems, Release 2.1* (Philadelphia, PA: SIAM)
Lehoucq R B, Sorensen D C and Yang C 1998 *ARPACK User's Guide: Solution of Large-Scale Eigenvalue Problems with Implicit Restarted Arnoldi Methods* (Philadelphia, PA: SIAM)

[16] Raymond S, Fafard S, Poole P J, Wójs A, Hawrylak P, Charbonneau S, Leonard D, Leon R, Petroff P M and Merz J L 1996 *Phys. Rev.* B **54** 11548
Raymond S, Hawrylak P, Gould P, Fafard S, Sachradja A, Potemski M, Wójs A, Charbonneau S, Leonard D, Petroff P M and Merz J L 1997 *Solid. State Commun.* **101** 883
[17] Bastard G 1988 *Wave Mechanics Applied to Semiconductor Heteroestructures* (Les Ulis: Les Éditions de Physique)
[18] Banin U, Lee C J, Guzelian A A, Kadavanich A V, Alivisatos A P, Jaskólski W, Bryant G W, Efros Al L and Rosen M 1998 *J. Chem. Phys.* **109** 2306
[19] Madelung O (ed) *Numerical Data and Functional Relationships in Science and Technology (Landolt-Börstein New Series Group III)* (Berlin: Springer)
[20] Xia J B 1989 *Phys. Rev.* B **40** 8500